IEEE Access
Multidisciplinary | Rapid Review | Open Access Journal

Received 27 May 2024, accepted 2 July 2024, date of publication 10 July 2024, date of current version 19 July 2024.

Digital Object Identifier 10.1109/ACCESS.2024.3426105

RESEARCH ARTICLE

A Multi-Terrain Robot Prototype With Archimedean Screw Actuators: Design, Realization, Modeling, and Control

ROZA GKLIVA[1], (Member, IEEE), WALID REMMAS[1,2], SIMON GODON[1], JAAN REBANE[1], KILIAN OCHS[1,3], MAARJA KRUUSMAA[1], AND ASKO RISTOLAINEN[1]

[1]Centre for Biorobotics, Department of Computer Systems, Tallinn University of Technology, 12618 Tallinn, Estonia
[2]Defsecintel Solutions OÃoe, 12618 Tallinn, Estonia
[3]Institute for Water and Environment (IWU), Karlsruhe Institute for Technology (KIT), 76131 Karlsruhe, Germany

Corresponding author: Roza Gkliva (roza.gkliva@taltech.ee)

This work was supported by the European Union's Research and Innovation Program Horizon 2020 Project ROBOMINERS under Grant 820971.

ABSTRACT This work introduces a robot prototype designed to explore locomotion, perception, and navigation in unstructured terrains. The focus of this paper is on the robot's locomotion, from concept design to realization, as well as modelling and control. The robot's locomotion system, comprising four individually controlled archimedean screw actuators, allows holonomic planar motion control. Testing on various yielding and hard grounds has demonstrated the system's efficacy. Additionally, 3-DOF kinematic and dynamic models were developed for pose estimation, control allocation, and numerical simulations on various terrains. Although dynamic models of archimedean screw locomotion systems have been proposed in the past, they have not been used for motion control or pose estimation. Experimental validation of the dynamic model demonstrates good performance for pose estimation, providing potential for future work on online model identification and model-based control. Furthermore, a trajectory tracking control scheme was evaluated on two distinct terrains, revealing valuable insights into the effectiveness and limitations of the proposed locomotion and trajectory tracking control scheme, and highlighting areas for future research.

INDEX TERMS Archimedean screw actuation, locomotion control, motion control, robot design, trajectory control.

I. INTRODUCTION

Ore mining is an industry with well-established historically profitable processes, but can be viewed as conservative regarding innovation [1]. In the last two decades, attempts have been made to increase the automation levels of mine operations [2], [3], [4], [5], [6]. The ROBOMINERS project [7] working in the same direction, aims to reduce the environmental impact and the risks to human operators [8]. One of the project's focus areas is the development of small-scale modular mining robots able to navigate and selectively mine ore in small deposits, which are usually unremunerative with conventional mining methods.

While the project's final prototype [9] is considered small-scale by mining industry standards, it is rather large from a robotics viewpoint. The development of such a robotic platform requires extensive testing to evaluate the feasibility and performance of its various components and algorithms and ensure reliable and robust operation in the hostile mining environment. In this context, we present the design, development and experimental evaluation of a robot prototype (Fig. 1) that can be used as a testing platform

The associate editor coordinating the review of this manuscript and approving it for publication was Wonhee Kim.

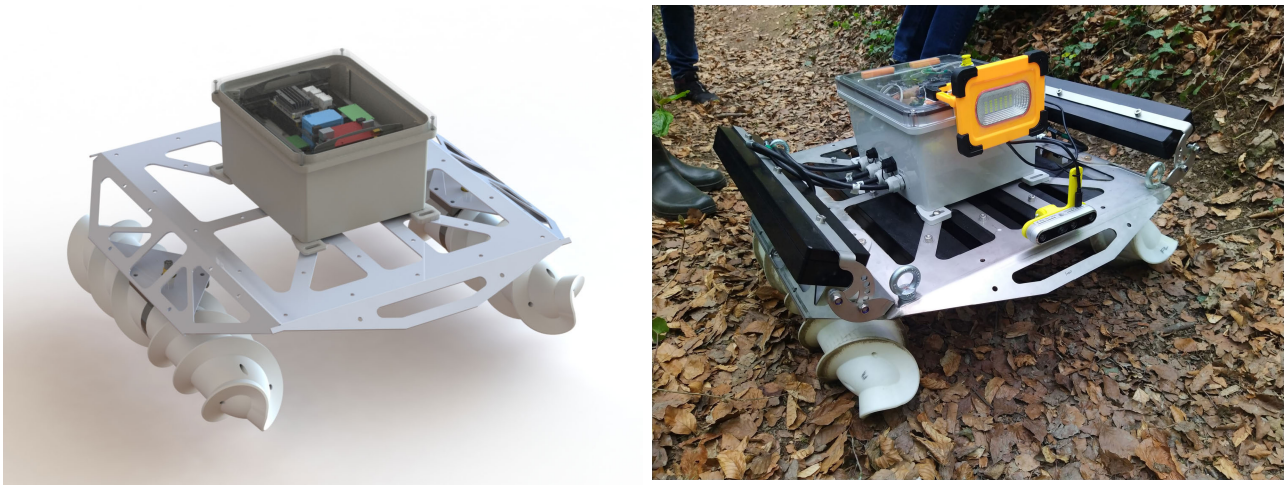

FIGURE 1. Robot CAD model and physical prototype.

for a variety of technologies related to the exploration of unstructured underground terrains, such as novel control, sensing, locomotion, and navigation methods. The reduced size and cost of this platform enable lower development costs and simplified logistics for experimental work. This paper focuses on the locomotion aspect of the prototype.

Modern mining machines commonly use tracks or very large wheels for locomotion through different types of media in the mining environment. Considering the reduced size of the proposed robot, these methods face issues related to mechanical complexity, large size and weight requirements, and reduced traction. While rare in literature, previous research showed that screw-based locomotion, despite being energetically inefficient on some terrains, can provide good traction in a variety of media [10], [11], [12], with reduced mechanical complexity compared to other locomotion mechanisms. For this reason, and due to the benefits stemming from the reduced number of moving parts and lower control requirements, the ROBOMINERS project is investigating the archimedean screw as a means of locomotion.

Previous investigations of archimedean screw-based locomotion include studies on modelling the interaction with the environment [13], or experimentally investigating the effect of varying screw parameters such as actuator dimensions, helix angle and height, etc. [14]. Several prototypes have been built using different configurations of screw actuators. An inline screw robot comprising four aligned screws [15] was used to investigate locomotion on soft terrain and push away soft obstacles. In [12] and [16], amphibian screw-driven robots that use two parallel screws are presented. Similarly, in [17], the authors modelled and built a two-screw-driven rover that moves on loose soil. A modular and reconfigurable screw-drive based robot was modelled and built in [18]. Other prototypes used four screws in an H-shaped configuration, where each screw can be independently controlled [11], and oriented [19]. Lastly, snake-like robots with screw actuators [20], [21], [22] have demonstrated different modes of locomotion for different terrains using reconfigurable robot body morphology.

TABLE 1. Prototype specifications.

Robot Dimensions	$0.79 \times 0.74 \times 0.43$ m
Total robot mass	29 kg
Actuator mass	6 kg
Electronics compartment mass	10 kg

This work presents a new robotic platform that uses four independently controlled archimedean screws for locomotion. Compared to designs described in the previous works, this configuration can achieve holonomic control on the plane while maintaining relatively low mechanical complexity. Both of these characteristics are integral to the robot's role as a small-scale and low-cost robust field robot.

While dynamic models of archimedean screw locomotion have been proposed in the past [17], [18], they have not been used for motion control or for pose estimation. In this work, we propose a dynamic model for the robot's locomotion system that can enhance its control and navigation capabilities. Lastly, we propose a trajectory tracking control scheme and experimentally demonstrate its effectiveness and limitations. To summarize, the contributions of this work include:

- **The design of a small-scale, robust mobile robot prototype**, that allows testing in challenging conditions with simplified logistics.
- **Control allocation for trajectory tracking, pose estimation, and simulations**, using an experimentally validated dynamic locomotion model.
- **Extensive experimental evaluation**, on yielding and hard terrains provides insights into the locomotion system and its control, and serves as proof-of-concept of the locomotion and modelling methods.

This paper is structured as follows: Section II introduces the proposed prototype. Section III presents the kinematics

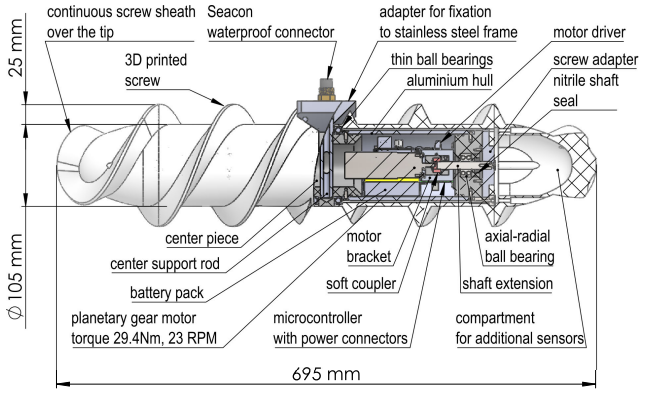

FIGURE 2. CAD model of actuator assembly.

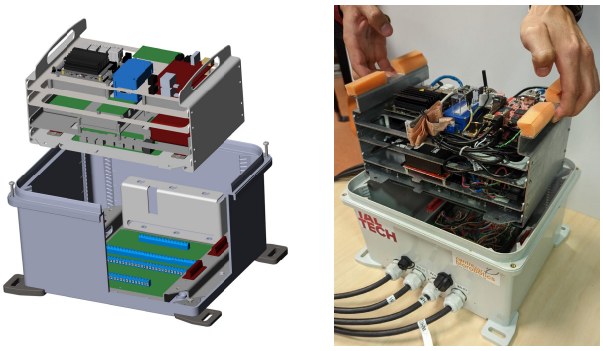

FIGURE 3. The main electronics compartment. Left: CAD model in section view. Right: physical prototype being assembled.

and dynamics of the robot. Section IV presents a trajectory tracking algorithm and its experimental evaluation, before concluding in Section V.

II. CONCEPT VEHICLE DESCRIPTION

This section describes the robot's hardware and software, comprising a combination of off-the-shelf and custom-made components. This vehicle is aimed to be used as a platform for the development and testing of technologies related to the exploration of unstructured environments. Its small size, low cost, and robust construction make it appropriate for use in rugged terrains outside of the laboratory without the challenging logistics that usually accompany such missions.

A. MECHANICAL DESIGN

The robot consists of four main parts: a rigid frame where other modules can be mounted, the main electronics compartment, and two locomotion modules positioned on either side of the robot (see Fig. 1). Design choices, such as the size and shape of the frame were made based on the robot's expected use as a testing platform. The robot's frame is made of 4 mm aluminium sheet, cut and bent to shape, with mounting holes for the robot's modules. The space between the actuators under the robot's body is planned to accommodate a variety of sensing systems that can analyze the substrate for selective mining and localization purposes. Information regarding the size and mass of the prototype can be found in Table 1. The main electronics compartment is a waterproof *Ensto* polycarbonate enclosure, mounted on the top side of the frame. Positioning the electronics compartment on top of the robot body raised the robot's centre of mass but did not negatively affect stability.

The robot's locomotion system comprises two actuators positioned at its sides, each consisting of two individually driven motor modules (Fig. 2). The two counter-rotating helices on each actuator allow to counteract the torque of the motor modules and enable isolated control of each DOF (Degree of Freedom). The number, positioning, and orientation of actuators were selected to allow holonomic control for 3-DOF planar motion and increased traction in wet and dry granular, as well as inclined terrains.

The actuator design parameters were derived from literature and adjusted based on an experimental evaluation of the generated force and efficiency as follows: the drum length to drum diameter ratio was set to approx.6 [14], two helix starts were selected for more dynamically stable operation [19], the helix angle was set to 30° for improved efficiency and thrust force [23]. The helix height was initially set to 1/8 of the drum diameter [14], but was doubled to 1/4 after initial testing demonstrated insufficient traction. The motor modules are housed in waterproof (IP68) canisters, made of anodized aluminium and polyoxymethylene (POM) parts. The outer screw is a Polylactic Acid (PLA) 3D-printed shell that is fixed to the motor shaft using a spider coupler. On its other end, towards the middle of the actuator, the shell is rotating on a bearing.

B. ELECTRONICS

In the main electronics enclosure (Fig. 3), a steel support frame with stacked plates can be lifted out for assembling or debugging. The plates hold different system components, such as two *A64-OLinuXino* single board computers by *Olimex*, one *Nvidia Jetson Nano* computer, batteries, networking devices, charging circuits, an *LGB304AE* Ethernet network switch, a PoE (Power over Ethernet) splitter combined with a custom *LM317*-based charging circuit for charging motor module batteries, as well as sensors such as a *BNO080* IMU, a *PI-48* IMU by *Pacific Inertial*, and an *MCP9808* temperature sensor. The connection between the liftable frame and the robot is through four *McMurdo D-Sub* backplane connectors. Waterproof connectors and cable glands are used to charge batteries and to connect external sensor and actuator modules. A magnet and reed switch pair enable power to the entire system with 5 V.

Each motor module is individually powered by an onboard battery pack consisting of five 18650 Lithium polymer cells connected in series. The battery pack can be charged through the main compartment when PoE power is present. Individual motor control is realised using a dedicated *Microchip ATmega328P*, and the motor control firmware

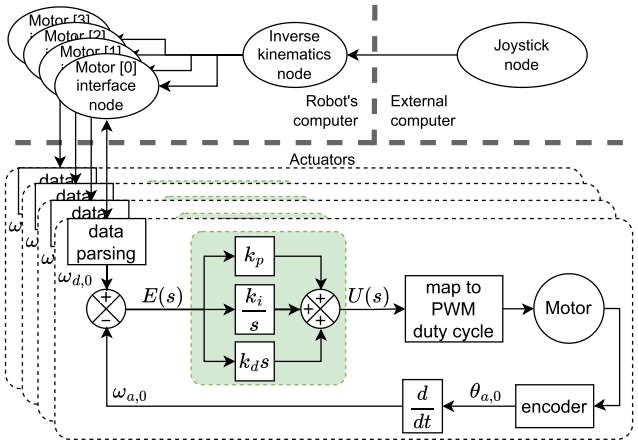

FIGURE 4. The robot's control system for remotely operated planar kinematic-based driving.

can be upgraded from one of the Olimex computers. Each motor (23 RPM HD Planetary gear motors with encoder by Servocity) is driven by a *Cytron MD20A* motor driver, powered directly from the motor module's onboard batteries. An *INA219* sensor is used to measure the current and voltage levels of each motor module.

C. SOFTWARE

The robot's locomotion control software is distributed across two layers (Fig. 4), with its parts running on several devices. The higher layer is implemented in an *A64-OlinuXino* computer, onboard the robot, running *ROS 2 Foxy* [24] on *Ubuntu 20.04*. High-level controller outputs result in actuator angular velocity commands, solving the kinematic and dynamic models described in Section III. On the actuator level, a discretized velocity-form PID controller implements velocity control in a 100 Hz control loop, as seen in Section IV-C. Each actuator is individually controlled and communicates with the high-level control via serial communication. The actual actuator velocity values $\omega_{a,i}$, $i \in [0, 3]$ are estimated by differentiating position feedback $\theta_{a,i}$, $i \in [0, 3]$ obtained with X4 decoding of the quadrature encoders output. The velocity estimation is transmitted back to the robot's computer, in a packet that also contains current and voltage measurements from the onboard *INA219* sensor. A simple *XOR* checksum algorithm is used to detect transmission errors, for both directions of communication between the robot's computer and the actuators. In the robot's computers, additional *ROS 2* nodes and other software utilities, not shown in Fig. 4, have been developed for data acquisition from the robot's onboard sensors.

III. MODELLING

Mathematical models of the robot allow us to simulate locomotion in conditions where it would be too challenging and dangerous to perform actual experiments. This section presents 3-DOF kinematic and dynamic models of the robot's locomotion and their experimental evaluation.

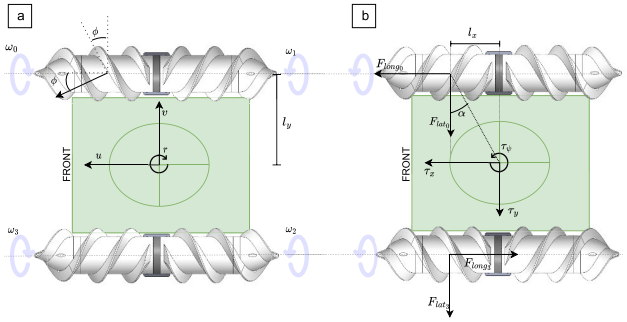

FIGURE 5. Illustration for mathematical model descriptions (a) kinematic model - bottom view, (b) dynamic model, top view. Clockwise rotation is considered positive in both models.

A. KINEMATIC MODEL

As the archimedean screw, similar to the mecanum wheel, generates tractive forces in both the longitudinal and lateral direction as it rotates, we extended the mecanum wheel model [11], [25], to account for the helix angle of the screw actuator. For the simplicity of this model, we assume that all actuators are in contact with the ground and that no slip occurs. The forward kinematic model (1) (Fig. 5a) is used to calculate the robot's planar body velocity $[u, v, r]^T$, using its actuators' angular velocities $\boldsymbol{\omega_i}$, $i \in [0, 3]$, and is used for basic simulation scenarios.

$$\begin{bmatrix} u & v & r \end{bmatrix}^T = r_s \boldsymbol{K_f} \begin{bmatrix} \omega_0 & \omega_1 & \omega_2 & \omega_3 \end{bmatrix}^T \tag{1}$$

Here, $r_s = 77.5$ mm is the screw actuator's radius including the helix, and the forward kinematic Jacobian matrix $\boldsymbol{K_f}$ is:

$$\boldsymbol{K_f} = \frac{1}{4} \begin{bmatrix} -\tan(\phi) & -\tan(\phi) & \tan(\phi) & \tan(\phi) \\ -1 & 1 & 1 & -1 \\ -1/\kappa & -1/\kappa & -1/\kappa & -1/\kappa \end{bmatrix}$$
$$\kappa = l_x + \frac{l_y}{\tan(\phi)} \tag{2}$$

where, $\phi = \pi/6$ rad is the helix angle, and $l_x = 0.15$ m, $l_y = 0.3$ m denote the distance between the motor module's geometrical centre and the robot's centre (Fig. 5a).

The inverse kinematic model (3) is used for the robot's locomotion, generating actuator velocity setpoints $\boldsymbol{\omega_i}$, $i \in [0, 3]$, from a body velocity input $[u, v, r]^T$, as

$$\begin{bmatrix} \omega_0 & \omega_1 & \omega_2 & \omega_3 \end{bmatrix}^T = \frac{1}{r_s} \boldsymbol{K_i} \begin{bmatrix} u & v & r \end{bmatrix}^T \tag{3}$$

where $\boldsymbol{K_i}$ is the inverse kinematic Jacobian matrix:

$$\boldsymbol{K_i} = \begin{bmatrix} -\frac{1}{\tan(\phi)} & -1 & -\kappa \\ -\frac{1}{\tan(\phi)} & 1 & -\kappa \\ \frac{1}{\tan(\phi)} & 1 & -\kappa \\ \frac{1}{\tan(\phi)} & -1 & -\kappa \end{bmatrix}. \tag{4}$$

While very simple and easy to implement for a human to drive the robot, due to the assumptions mentioned above, the kinematic model is quite inaccurate and unreliable for

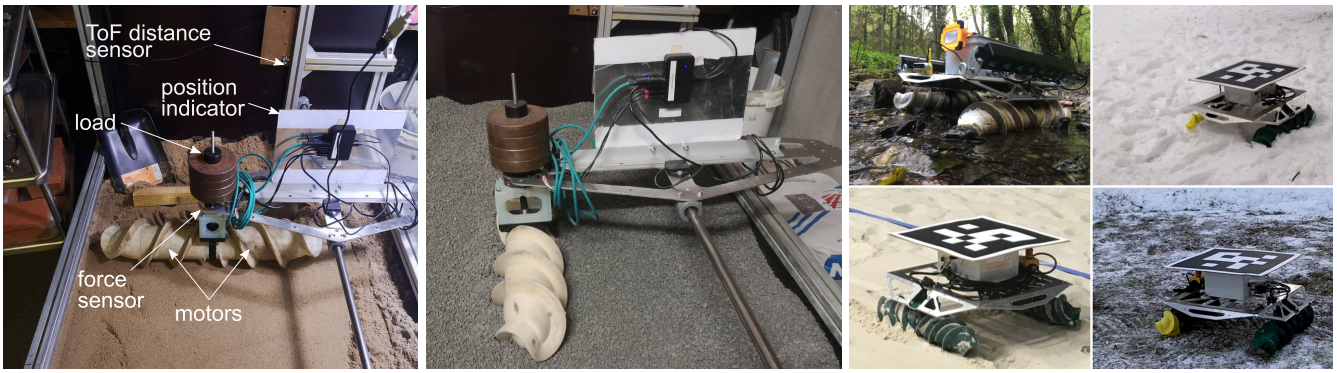

FIGURE 6. Experimental setups for the model identification and validation: (a) Measurement of lateral forces during lateral motion on sand, (b) Measurement of longitudinal forces during longitudinal motion on gravel. (c) The robot during experiments on various terrains (mud, snow, sand, frozen ground).

autonomous control. For this reason, a dynamic model was derived, that can compensate for the slippage between the actuators and the terrain.

B. DYNAMIC MODEL

The proposed model is developed with the objective of estimating the robot's pose in the world frame $\boldsymbol{\eta} = [x, y, \psi]^T$, based on its velocities in the robot frame $\boldsymbol{\zeta} = [u, v, r]^T$. The actuator forces generated by the screws' interaction with the ground are denoted by $\boldsymbol{\tau} = [\tau_x, \tau_y, \tau_\psi]^T$. We hypothesize that within the studied screw velocity ranges, the generated force $\boldsymbol{\tau}$ varies proportionally to the corresponding screw velocities $\boldsymbol{\omega} = [\omega_0, \omega_1, \omega_2, \omega_3]^T$. Moreover, we assume that the robot is subject to linear friction forces $\boldsymbol{D} = diag([D_x, D_y, D_\psi])$. Non-linear friction forces are neglected as the robot operates at a very low speed.

The dynamic model is defined as below:

$$\dot{\boldsymbol{\eta}} = \boldsymbol{J}(\boldsymbol{\eta})\boldsymbol{\zeta} \tag{5}$$

$$\boldsymbol{M}\dot{\boldsymbol{\zeta}} = -\boldsymbol{D}\boldsymbol{\zeta} + \boldsymbol{\tau} \tag{6}$$

$$\boldsymbol{\tau} = \boldsymbol{\sigma}\boldsymbol{B}\boldsymbol{\omega} \tag{7}$$

Here, $\boldsymbol{M}$ (3×3) is the rigid body mass matrix of the robot such that

$$\boldsymbol{M} = \begin{bmatrix} m & 0 & 0 \\ 0 & m & 0 \\ 0 & 0 & I_z \end{bmatrix}, \tag{8}$$

where m denotes the homogeneous mass of the robot, and I_z represents the moment of inertia about its z-axis. $\boldsymbol{J}(\boldsymbol{\eta})$ (3×3) is a rotation matrix that transforms velocities from body to world frame, such that:

$$\boldsymbol{J}(\boldsymbol{\eta}) = \begin{bmatrix} cos(\psi) & -sin(\psi) & 0 \\ sin(\psi) & cos(\psi) & 0 \\ 0 & 0 & 1 \end{bmatrix}, \tag{9}$$

and $\boldsymbol{B}$ (3×4) is the control allocation matrix that relates the screw velocities $\boldsymbol{\omega}$ to body forces $\boldsymbol{\tau}$. We assume that each screw generates a longitudinal force F_{long} and a lateral force F_{lat} (as shown in Fig. 5b) which are computed based on the screw velocities $\boldsymbol{\omega}$ and a set of parameters $\boldsymbol{\sigma}$ defined as $diag([\sigma_{long}, \sigma_{lat}, \sigma_{lat}])$. The parameters σ_{long} and σ_{lat} are identified experimentally. Finally, the allocation matrix $\boldsymbol{B}$ is defined as:

$$\boldsymbol{B} = \begin{bmatrix} -1 & -1 & -l_x sin(\alpha) \\ -1 & 1 & -l_x sin(\alpha) \\ 1 & 1 & -l_x sin(\alpha) \\ 1 & -1 & -l_x sin(\alpha) \end{bmatrix}^T, \tag{10}$$

with $l_x = 0.15$ m and the angle of the lever arm $\alpha = 26.5°$.

C. MODEL VALIDATION

This section details the experimental setup that was employed to identify and validate the dynamic model of the robot. To identify the parameters σ_{long} and σ_{lat}, we mounted one actuator on a gantry (Fig. 6a,b) to achieve either a longitudinal or a lateral motion, and measured respectively the generated forces F_{long} and F_{lat}. An additional load of 10 kg was added on top of the actuator, to approximate the load each actuator carries when the robot is assembled. Each scenario was repeated 10 times for three screw velocities, 5 rpm, 10 rpm and 20 rpm, on two types of terrains, namely sand, and $2 - 6$ mm granite gravel. For each experiment, the screw module moved about 0.5 m along the gantry's rail length, and the following variables were measured at a frequency of 100 Hz:

- The generated forces, using an *ATI Axia80-M20* force-torque sensor.
- The screw module displacement along the gantry rail, using an *Adafruit VL53L0X* Time-of-Flight (ToF) sensor.
- The screw rotational velocities ω_0 and ω_1, calculated using the motors' encoders.

Since only the screw module was used instead of the whole robot, with a constraint to move only in one DOF, the reduced

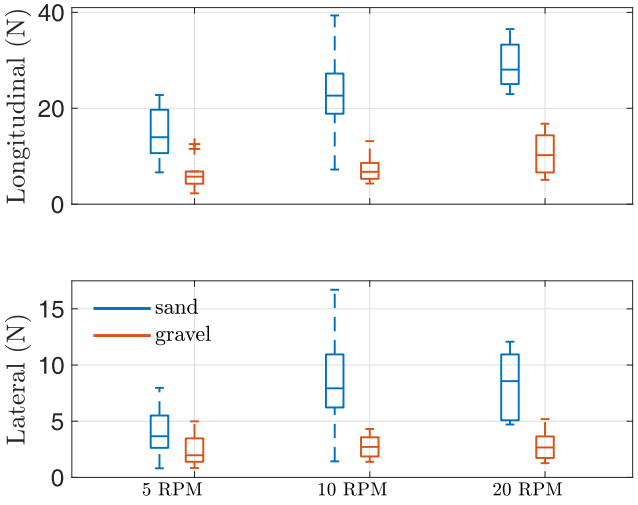

FIGURE 7. Whisker plot of the measured mean longitudinal and lateral forces.

dynamic model for longitudinal motion becomes:

$$\ddot{x} = \frac{-D_x u + \tau_x}{m_{screw} + m_{load}} \tag{11}$$

$$\tau_x = \sigma_{long} \boldsymbol{B_x} \boldsymbol{\omega_s} \tag{12}$$

and the reduced dynamic model for lateral motion becomes:

$$\ddot{y} = \frac{-D_y v + \tau_y}{m_{screw} + m_{load}} \tag{13}$$

$$\tau_y = \sigma_{lat} \boldsymbol{B_y} \boldsymbol{\omega_s} \tag{14}$$

such that $\boldsymbol{B_x} = [-1, -1]$, $\boldsymbol{B_y} = [-1, 1]$ and $\boldsymbol{\omega_s} = [\omega_0, \omega_1]^T$. To identify the parameters σ_{long} and σ_{lat}, we construct the linear regressor $\boldsymbol{Y_\sigma} = \boldsymbol{X_\sigma} \boldsymbol{\beta_\sigma} + \boldsymbol{\epsilon}$, such that:

$$\boldsymbol{Y_\sigma} = \begin{bmatrix} F_{long_0} & 0 \\ \vdots & \vdots \\ F_{long_n} & 0 \\ 0 & F_{lat_0} \\ \vdots & \vdots \\ 0 & F_{lat_n} \end{bmatrix}, \boldsymbol{X_\sigma} = \begin{bmatrix} \boldsymbol{B_x}\omega_{s_0} & 0 \\ \vdots & \vdots \\ \boldsymbol{B_x}\omega_{s_n} & 0 \\ 0 & \boldsymbol{B_y}\omega_{s_0} \\ \vdots & \vdots \\ 0 & \boldsymbol{B_y}\omega_{s_n} \end{bmatrix} \tag{15}$$

and $\boldsymbol{\beta_\sigma} = diag([\sigma_{long}, \sigma_{lat}])$. The least square estimator $\hat{\boldsymbol{\beta}}_\sigma = diag([\hat{\sigma}_{long}, \hat{\sigma}_{lat}])$ is then computed as follows:

$$\hat{\boldsymbol{\beta}}_{\boldsymbol{\sigma}} = (\boldsymbol{X_\sigma}^T \boldsymbol{X_\sigma})^{-1} \boldsymbol{X_\sigma}^T \boldsymbol{Y_\sigma} \tag{16}$$

Fig. 7 illustrates the averaged longitudinal and lateral forces on sand and gravel at various velocities. These measured forces validate that increasing the screw velocity within the observed range leads to an augmentation in force generation in both longitudinal and lateral directions. The higher variability of measurements observed at the 10 rpm sets is due to a resonance effect that increased the vibrations of the test setup during these experiments. Additionally, it is noted that the screw-module exhibits significantly greater force generation on sand terrains than on gravel ones.

TABLE 2. Coefficients for the screw module experiments.

	D_x	D_y	m_{screw} (Kg)	m_{load} (Kg)
Sand	529.95	76.1307	6	10
Gravel	214.78	23.52	6	10

TABLE 3. Coefficients used for the model validation experiments.

	D_x	D_y	D_ψ	m (Kg)	I_z $(Kg.m^2)$
Frozen grass	509.81	210.50	4.52	29	3.72
Sand	560.33	320.08	11.46	29	3.72

TABLE 4. RMS errors of pose estimation on different terrains and RPM speeds.

	Sand			Frozen grass		
	x (m)	y (m)	ψ (rad)	x (m)	y (m)	ψ (rad)
$5RPM$	0.020	0.040	0.040	0.049	0.038	0.047
$10RPM$	0.022	0.029	0.047	0.037	0.040	0.107
$15RPM$	0.045	0.030	0.069	0.0192	0.022	0.064

The data depicted in Fig. 7 was sorted to compute the parameters of $\hat{\boldsymbol{\beta}}_\sigma$ for both sand and gravel separately using (16). The resulting values are $\sigma_{long} = 0.812$ and 0.297, and $\sigma_{lat} = 0.247$ and 0.0853 for sand and gravel respectively.

With the assumption of constant velocity, the parameters D_x and D_y can also be identified using the linear regressor $\boldsymbol{Y_D} = \boldsymbol{X_D} \boldsymbol{\beta_D} + \boldsymbol{\epsilon}$, such that:

$$\boldsymbol{Y_D} = \begin{bmatrix} \tau_{x_0} & 0 \\ \vdots & \vdots \\ \tau_{x_n} & 0 \\ 0 & \tau_{y_0} \\ \vdots & \vdots \\ 0 & \tau_{y_n} \end{bmatrix}, \boldsymbol{X_D} = \begin{bmatrix} u_0 & 0 \\ \vdots & \vdots \\ u_n & 0 \\ 0 & v_0 \\ \vdots & \vdots \\ 0 & v_n \end{bmatrix} \tag{17}$$

where the values of τ_{x_i} and τ_{y_i} for $i = 0..n$ are computed using (12) and (14) respectively, and the velocities u_i and v_i are derived from differentiating the measured displacement.

To validate the identified dynamic model for the screw actuator, we compare its measured velocity along the gantry to its estimated velocity using the identified parameters. The identified friction parameters D_x and D_y are denoted in Table 2. Fig. 8 shows the results for all trials on sand and on gravel.

The findings indicate that the proposed model can effectively estimate the longitudinal and lateral velocities of the screw on different terrain types. Moreover, the results reveal that the robot's movement speed is similar on both terrains within the studied range of screw velocities, despite the fact that the force generation in the screw module is higher on sand (Fig. 7). Additionally, the identified friction parameters suggest that the robot encounters greater resistance on sand.

To identify the dynamic model for the robot, we conducted an additional scenario where the robot was equipped with a 53 cm ArUco marker (cf. Fig 6c) and, using the kinematic model, was driven on two different terrains, namely sand and frozen grass. These two terrains serve as test cases for

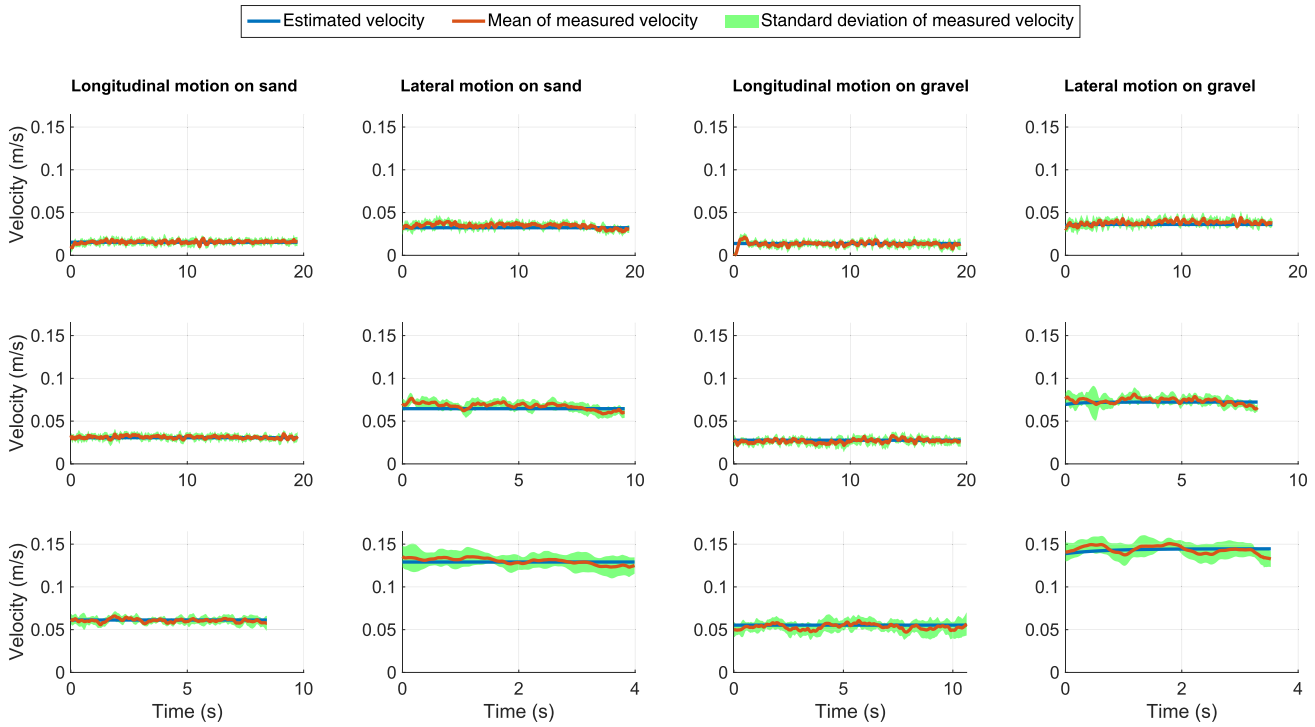

FIGURE 8. Estimated and measured velocities on sand and gravel during longitudinal and lateral motion: Top: 5 rpm, middle: 10 rpm, bottom: 20 rpm.

locomotion on very low and high-yield terrains. The robot's pose was visually measured using an external camera that tracked the robot's pose from above. The robot's motion was controlled along all its individual DOFs at three different actuator speeds: 5 rpm, 10 rpm, and 15 rpm. Each experiment was repeated five times to ensure consistency of results.

To identify the robot's friction parameters, we used the same method based on linear regression as in the previous experiments. In addition to D_x and D_y, an additional parameter D_ψ was included to account for rotational friction. The identified numeric values are summarized in Table 3. Since the parameters σ were not identified for the frozen grass terrain, tentative values of $\sigma_{long} = 0.4$ and $\sigma_{lat} = 0.16$ were chosen. The selected tentative values were justified based on the best available knowledge and understanding of the terrain properties, and were within the previously identified ranges.

To evaluate the precision of the proposed model, we analyzed the root mean square (RMS) errors between the measured and estimated poses of the robot while it moved along its controllable DOFs, namely x, y, and heading ψ. The outcomes of this analysis are presented in Table 4. The findings demonstrate that the identified dynamic model is able to accurately estimate the robot's pose when it moves independently along each DOF. Moreover, the results indicate that the identified friction parameters $\boldsymbol{D}$ can compensate for the lack of knowledge of the exact value of σ, as evidenced by the accuracy of the RMS errors.

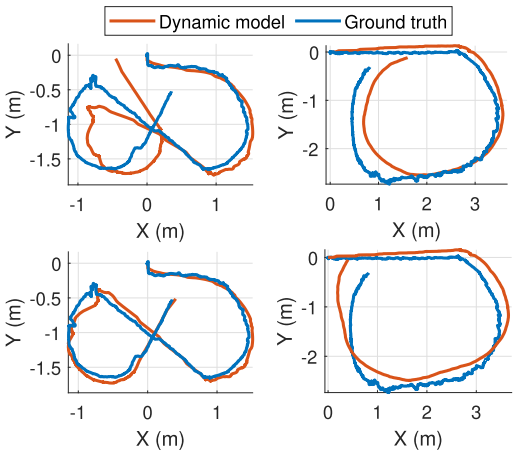

FIGURE 9. Experimental results for the measured and estimated position of the robot on frozen grass (left) and on sand (right) (see Fig. 6c). The top plots show the estimated position based solely on the model, while the bottom plots show the estimated position with heading correction using the IMU.

To test the model's accuracy when moving with more than one DOF at a time, the robot was driven manually on both sand and frozen grass. Its position was visually measured using an external camera that tracked the robot's pose from above. The results are illustrated in Fig. 9. These results demonstrate that pose estimation relying solely on the proposed model is subject to drift. This drift is potentially due to varying quality of traction that causes the model's accuracy to fluctuate, and error to accumulate over time. One way to

mitigate this drift and enhance the estimation results is to correct the heading of the robot based on IMU orientation measurements. This approach can effectively improve the accuracy of the pose estimation. While in this case, the IMU orientation directly replaced the model-based orientation estimation, in the future, a Kalman filter-based approach can be used for the fusion of model-based and sensor-based estimations.

IV. TRAJECTORY TRACKING

In this section, we present the trajectory tracking control scheme for the proposed robot, motivated by the need to evaluate its performance for 3-DOF trajectory tracking across different terrains.

To begin, we introduce a trajectory generation approach that ensures the robot can execute smooth and feasible trajectories. We then describe the control laws, which are implemented on the robot. While this study primarily examines the performance of a baseline controller, the primary intention behind these experiments is to establish a comprehensive framework for testing and evaluating diverse control strategies for the screw-driven robot.

A. TRAJECTORY GENERATION

The trajectory to be followed is produced using a second-order Ordinary Differential Equation (ODE) represented by:

$$\ddot{\boldsymbol{\eta}}_d + 2\gamma\dot{\boldsymbol{\eta}}_d = \gamma^2(\boldsymbol{\eta_d} - \boldsymbol{\eta_p}) \tag{18}$$

The ODE filter is designed to generate velocities and accelerations that are smooth, continuous, and feasible, even in the presence of non-linearities in the desired set points. To obtain the desired states, i.e., η_d, $\dot{\eta}_d$, and $\ddot{\eta}_d$, a double Euler integration is performed.

The ODE filter leverages a collection of pre-filtered set-points, denoted by $\boldsymbol{\eta_p} = [x_p, y_p, \psi_p]$, to create a continuous sequence of desired poses $\boldsymbol{\eta_d} = [x_d, y_d, \psi_d]$, velocities $\dot{\boldsymbol{\eta}}_d = [\dot{x}_d, \dot{y}_d, \dot{\psi}_d]$, and accelerations $\ddot{\boldsymbol{\eta}}_d = [\ddot{x}_d, \ddot{y}_d, \ddot{\psi}_d]$.

B. TRAJECTORY TRACKING CONTROLLER

To assess the ability of the screw-actuated robot to accurately follow a desired trajectory, we employed a conventional Proportional-Integral-Derivative (PID) controller. The tracking error and its derivative were defined as:

$$\tilde{\boldsymbol{\eta}} = \boldsymbol{\eta_d} - \boldsymbol{\eta} \tag{19}$$

$$\tilde{\boldsymbol{\xi}} = \boldsymbol{J}^{-1}\dot{\boldsymbol{\eta}}_d - \boldsymbol{\xi} \tag{20}$$

Here, $\boldsymbol{\eta_d}$ denotes the desired pose, $\boldsymbol{\eta}$ is the actual pose measured with the external camera, and $\boldsymbol{\xi}$ represents the actual velocity. The linear velocity $[u, v]$ is computed by differentiating the measured $[x, y]$ position, and the angular velocity r is measured using the robot's onboard IMU. Finally, The control input is represented by the equation:

$$\boldsymbol{\tau_{PID}} = \boldsymbol{K_p}\tilde{\boldsymbol{\eta}} + \boldsymbol{K_d}\tilde{\boldsymbol{\xi}} + \boldsymbol{K_i}\int_0^{t_1}\tilde{\boldsymbol{\eta}}(t)dt \tag{21}$$

TABLE 5. PID Coefficients employed for trajectory tracking.

	K_p	K_d	K_i
Frozen grass	160	90	1.5
Sand	150	30	1.2

In this equation, $\boldsymbol{K_p}$, $\boldsymbol{K_d}$, and $\boldsymbol{K_i}$ are diagonal positive-definite matrices of dimensions 3×3 that regulate the proportional, derivative, and integral gains, respectively. The values of these parameters were manually tuned via a trial-and-error method. The corresponding numerical values of the tuned parameters are listed in Table 5.

The identified dynamic model is utilized to convert the controller output signals to screw velocities using the pseudo-inverse of the allocation matrix $\boldsymbol{\sigma B}$, as depicted by the following equation:

$$\boldsymbol{\omega} = (\boldsymbol{\sigma B})^{\dagger}\boldsymbol{\tau_{PID}} \tag{22}$$

C. ACTUATOR CONTROL

For control of each actuator's angular velocity, a discretized, velocity-form PID [26] was implemented, as it is particularly suited for implementation in a microcontroller, and has built-in anti-windup [26, pp.82]. The velocity form of the controller is calculated using its output u_k and u_{k-1} at times k and $k-1$ respectively.

$$u_k = u_{k-1} + e_k A + e_{k-1}B + e_{k-2}C, \tag{23}$$

$$A = k_p + \frac{k_i T}{2} + \frac{k_d}{T},$$

$$B = -k_p + \frac{k_i T}{2} - 2\frac{k_d}{T},$$

$$C = \frac{k_d}{T} \tag{24}$$

Here, e_k, e_{k-1}, and e_{k-2} denote the angular velocity errors for times k, $k-1$, and $k-2$. Equations (23) and (24) are implemented in the motor module microcontroller. (23) is solved at 100 Hz rate and the constants A, B, and C in (24) are calculated by the C preprocessor. The controller gains $k_p = 0.5$, $k_i = 0.0003$ and $k_d = 0.005$ were empirically tuned.

D. CONTROLLER EVALUATION - RESULTS

The trajectory tracking performance of the robot on frozen grass and sand terrains was investigated, and the results are presented in Fig. 10. The findings reveal that the robot can accurately track a reference trajectory in 3-DOF on hard terrains such as frozen grass, which present less maneuverability restrictions. This performance can be attributed to the trajectory tracking control scheme that involves the inverse dynamic model presented in (22). This allowed accurate force allocation among the robot's actuators to move precisely along the reference trajectory.

However, the results in Fig. 10b indicate that the robot's trajectory tracking performance is not as precise on sand.

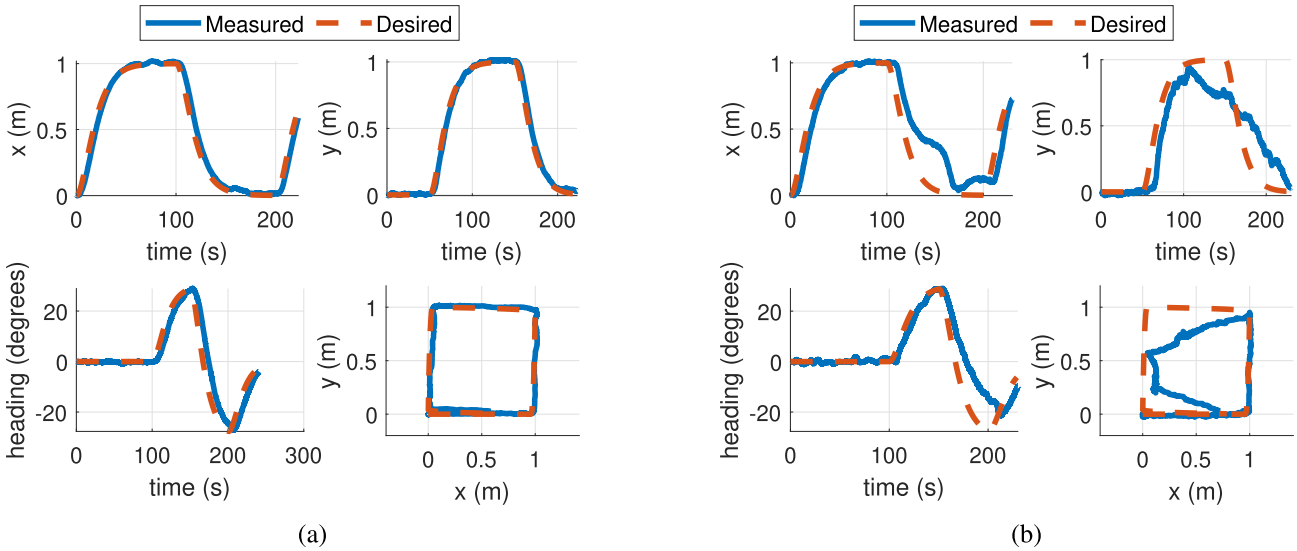

FIGURE 10. Trajectory tracking results on (a) hard (frozen grass) and on (b) low-yield (sand) terrain.

The primary reason for this discrepancy is that the robot was unable to move diagonally along the actuator's helix angle (30°) on sand terrain. To enable this diagonal motion, only two diagonally opposed screws were actuated while the other two were stopped. This resulted in the robot being blocked due to the high friction that was too difficult to overcome with only two actuators in motion. This issue arises primarily from the use of the pseudo-inverse in (22), resulting in an equitable distribution of forces. However, this approach does not favour optimal conditions for diagonal movement on sandy terrain. As indicated in (10), the matrix $\boldsymbol{B}$ is of full rank 3, and the system has more actuators than DOFs, which indicates that the system is over-actuated and the allocation system possesses theoretically infinite potential solutions. Therefore, forthcoming research should explore more refined strategies for solving the inverse allocation system, with a particular focus on enhancing diagonal mobility. These findings highlight the limitations and challenges of achieving accurate trajectory tracking on challenging terrains. This emphasizes the need for further investigations on the control level to address motion restrictions on terrains such as sand.

V. DISCUSSION AND CONCLUSION

In this work, we presented the design, modelling, and experimental evaluation of a robot prototype, which uses archimedean screw actuators for locomotion on a variety of terrains. The motivation for this work was the investigation of technologies related to the exploration of unstructured underground environments, as part of the ROBOMINERS [7] project. The small size and lower fabrication cost of this prototype simplify logistics for experimental work, which allows us to draw accurate conclusions that can be scaled-up to the final ROBOMINERS prototype [9]. The experiments presented in this paper and in the accompanying video, demonstrate the robustness of the robot's design. Despite having some 3D printed parts, the locomotion system performs well in a variety of terrains and conditions, ranging from grassy and granular, to muddy and rocky, flat and inclined terrains. Despite the vibrations and harsh motions associated with locomotion in unstructured environments, the robot's actuation, data acquisition, power, and communications remain reliable. The robot's modular design allows easy reconfiguration of hardware and software, that can enable investigation of different actuator, sensor, and computing configurations. This feature allowed the separate investigation of the dynamics of the individual screw actuator and of the full robot, for identification and validation of the dynamic model. During the development and demonstrations of the final prototype [27] of the ROBOMINERS project, the findings of this work were instrumental for the design and implementation of locomotion control schemes.

The initial experiments with the robot were focused on developing and validating a reliable dynamic model. The results show that the dynamic model is effective for pose estimation, especially after orientation corrections using IMU measurements. In this work it enabled online pose estimation, and was used to perform control allocation for trajectory tracking scenarios. The dynamic model has potential for more accurate simulations, which can enable future testing of complex robot behaviours in simulation and on field, such as model-based locomotion control strategies, negotiating locomotion in hostile environments, etc.

Future work includes extending the dynamic model for all DOFs, which would enable more accurate pose estimation for non-flat terrains. Additionally, the robot's locomotion can be augmented by increasing the DOFs of its actuators with additional joints that can control the orientation of the actuators and/or motor modules. Related to the robot's autonomy, future work will investigate trajectory generation

methods that can produce terrain-specific feasible trajectories based on the introduced dynamic model. Lastly, this platform will continue to be used for its intended purpose, as a testing platform for novel methods and technologies for negotiating uncertain environments [28], expanding to perception, localization and mapping strategies.

ACKNOWLEDGMENT

The authors thank the ROBOMINERS consortium partners for the very fruitful discussions.

(Roza Gkliva and Walid Remmas contributed equally to this work.)

REFERENCES

[1] F. Sánchez and P. Hartlieb, "Innovation in the mining industry: Technological trends and a case study of the challenges of disruptive innovation," *Mining, Metall. Explor.*, vol. 37, no. 5, pp. 1385–1399, Oct. 2020.

[2] P. G. Ranjith, J. Zhao, M. Ju, R. V. S. De Silva, T. D. Rathnaweera, and A. K. M. S. Bandara, "Opportunities and challenges in deep mining: A brief review," *Engineering*, vol. 3, no. 4, pp. 546–551, Aug. 2017.

[3] B. Siciliano, O. Khatib, and T. Kröger, *Springer Handbook of Robotics*. Berlin, Germany: Springer, 2008.

[4] L. Bołoz and W. Biały, "Automation and robotization of underground mining in Poland," *Appl. Sci.*, vol. 10, no. 20, p. 7221, Oct. 2020.

[5] J. Ralston, D. Reid, C. Hargrave, and D. Hainsworth, "Sensing for advancing mining automation capability: A review of underground automation technology development," *Int. J. Mining Sci. Technol.*, vol. 24, no. 3, pp. 305–310, May 2014.

[6] M. N. Wendt and G. A. Einicke, "Development of a water-hydraulic self-propelled robotic drill for underground mining," in *Field and Service Robotics*. Berlin, Germany: Springer, 2006, pp. 355–366.

[7] *Robominers*. Accessed: May 24, 2024. [Online]. Available: https://robominers.eu/

[8] L. Lopes, B. Bodo, C. Rossi, S. Henley, G. Žibret, A. Kot-Niewiadomska, and V. Correia, "ROBOMINERS—Developing a bio-inspired modular robot-miner for difficult to access mineral deposits," *Adv. Geosci.*, vol. 54, pp. 99–108, Oct. 2020.

[9] J. Aaltonen, K. Koskinen, J. Laitinen, E. Friman, K. Hakonen, T. Salomaa, and P. Ulmanen, "ROBOMINERS deliverable 3.1 system requirements: Robominer requirement specification," Dept. Automat. Technol. Mech. Eng., Tampere Univ., Tampere, Finland, Tech. Rep., Oct. 2020.

[10] S. J. Knight, E. S. Rush, and B. G. Stinson, "Trafficability tests with the Marsh screw amphibian," *J. Terramechanics*, vol. 2, no. 4, pp. 31–50, Jan. 1965.

[11] J. H. Lugo, V. Ramadoss, M. Zoppi, and R. Molfino, "Conceptual design of tetrad-screw propelled omnidirectional all-terrain mobile robot," in *Proc. 2nd Int. Conf. Control Robot. Eng. (ICCRE)*, Apr. 2017, pp. 13–17.

[12] T. W. Koepenick, "Surf-zone underwater robotic demonstration platform," Applied Res. Associates, Albuquerque NM, USA, Tech. Rep. ADA607840, 2014.

[13] R. Lotman and M. A. Grima, "Deep sea mining with an archimedes screw driven vehicle," in *Proc. Int. Conf. Offshore Mech. Arctic Eng.*, vol. 44373, 2011, pp. 113–120.

[14] H. Dugoff and I. Robert Ehlich, "Model tests of bouyant screw rotor configurations," *J. Terramechanics*, vol. 4, no. 3, pp. 9–22, Jan. 1967.

[15] K. Matsuhiro, K. Tanaka, S. Inoue, T. Zhong, K. Kida, Y. Sugahara, A. Takanishi, and H. Ishii, "Development of small robot with inline Archimedean screw mechanism that can move through wetlands," in *Proc. Symp. Robot Design, Dyn. Control*, Sapporo, Japan. Cham, Switzerland: Springer, Sep. 2020, pp. 338–346.

[16] L. Ju, G. Ferri, C. Laschi, B. Mazzolai, and P. Dario, "Experimental results of a novel amphibian solution for aquatic robot," in *Proc. IEEE Int. Conf. Robot. Autom.*, May 2010, pp. 2261–2266.

[17] K. Nagaoka and T. Kubota, "Modeling and analysis on exploration rover with screw drive mechanism over loose soil," in *Proc. 10th Int. Symp. Artif. Intell., Robot. Automat. Space*, 2010, pp. 162–169.

[18] J. Liedke, L. Winkler, and H. Wörn, "An alternative locomotion unit for mobile modular self-reconfigurable robots based on archimedes screws," in *Proc. 9th Int. Symp. Mechatronics Appl. (ISMA)*, Apr. 2013, pp. 1–6.

[19] J. T. Freeberg, "A study of omnidirectional quad-screw-drive configurations for all-terrain locomotion," M.S. thesis, Dept. Mech. Eng., College Eng., Univ. South Florida, Tampa, FL, USA, 2010.

[20] D. A. Schreiber, F. Richter, A. Bilan, P. V. Gavrilov, H. M. Lam, C. H. Price, K. C. Carpenter, and M. C. Yip, "ARCSnake: An Archimedes' screw-propelled, reconfigurable serpentine robot for complex environments," in *Proc. IEEE Int. Conf. Robot. Autom. (ICRA)*, May 2020, pp. 7029–7034.

[21] R. Thakker, M. Paton, M. P. Strub, M. Swan, G. Daddi, R. Royce, P. Tosi, M. Gildner, T. Vaquero, and M. Veismann, "EELS: Towards autonomous mobility in extreme terrain with a versatile snake robot with resilience to exteroception failures," in *Proc. IEEE/RSJ Int. Conf. Intell. Robots Syst. (IROS)*, Oct. 2023, pp. 9886–9893.

[22] T. Vaquero, G. Daddi, R. Thakker, M. Paton, A. Jasour, M. Strub, R. Swan, R. Royce, M. Gildner, and P. Tosi, "EELS: Autonomous snake-like robot with task and motion planning capabilities for ice world exploration," *Sci. Robot.*, vol. 9, no. 88, Mar. 2024, Art. no. eadh8332.

[23] B. Cole, "Inquiry into amphibious screw traction," *Proc. Inst. Mech. Eng.*, vol. 175, no. 1, pp. 919–940, 1961.

[24] S. Macenski, T. Foote, B. Gerkey, C. Lalancette, and W. Woodall, "Robot operating system 2: Design, architecture, and uses in the wild," *Sci. Robot.*, vol. 7, no. 66, May 2022, Art. no. eabm6074.

[25] P. Viboonchaicheep, A. Shimada, and Y. Kosaka, "Position rectification control for Mecanum wheeled omni-directional vehicles," in *Proc. 29th Annu. Conf. IEEE Ind. Electron. Soc.*, Nov. 2003, pp. 854–859.

[26] T. Hagglund and K. J. Astrom, *PID Controllers: Theory, Design, and Tuning*, ch. 3, 1995, pp. 59–119.

[27] *ROBOMINERS*. Accessed: May 24, 2024. [Online]. Available: https://robominers.eu/2023/09/11/robominers-field-trials-in-estonia-audio-visual-coverage/

[28] T. Kossas, W. Remmas, R. Gkliva, A. Ristolainen, and M. Kruusmaa, "Whisker-based tactile navigation algorithm for underground robots," in *Proc. IEEE Int. Conf. Robot. Autom. (ICRA)*, May 2024, pp. 13164–13170.

ROZA GKLIVA (Member, IEEE) received the B.Sc. degree in mechanical engineering and the M.Sc. degree in advanced systems in manufacturing, automation and robotics from the Technological Educational Institute of Crete, Greece, in 2010 and 2016, respectively, and the Ph.D. degree in computer and systems engineering from Tallinn University of Technology (TalTech), Estonia, in 2023. She is currently a Researcher with the Centre for Biorobotics, TalTech. Her research interests include underwater and amphibious robot locomotion, soft robotics, and embedded control systems.

WALID REMMAS received the M.Sc. degree in control system engineering from the Polytechnic School of Constantine, Algeria, in 2017, the M.Sc. degree in robotics from the University of Montpellier, France, in 2018, and the joint Ph.D. degree in computer and systems engineering from Tallinn University of Technology, Estonia, and the University of Montpellier, in 2023. He is currently a Researcher with Defsecintel Solutions, where he continues to contribute to advancements in computer vision and control. His research interests include intelligent control, underwater robotics, and computer vision.

SIMON GODON received the B.Sc. and Diplôme d'Ingénieur (equivalent to M.Eng.) degrees from Arts et Métiers ParisTech, France, in 2019, and the M.Sc. degree in robotics from the University of Bristol, U.K., in 2019. He is currently pursuing the Ph.D. degree in robotics with Tallinn University of Technology (TalTech), Estonia. His research interests include legged robotics and locomotion in complex and yielding environments.

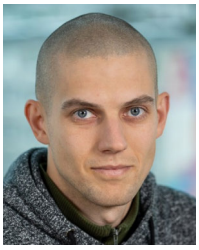

JAAN REBANE received the B.Sc. degree in electronics and the M.Sc. degree in electronics and bionics from Tallinn University of Technology (TalTech), Estonia, in 2008 and 2010, respectively. Since then, he has been an Engineer with the Centre for Biorobotics, TalTech, building electrical systems in robots, as well as stand-alone environmental sensors.

KILIAN OCHS received the B.Sc. degree in integrated engineering and the M.Sc. degree in computer and systems engineering from Tallinn University of Technology (TalTech), Estonia, in 2018 and 2020, respectively. During the master's studies and after his graduation, he was with the Centre for Biorobotics, TalTech, mainly improving the usability of certain bioinspired underwater AUVs. Since 2022, he has been a Specialist in measurement and control with the Institute for Water and Environment (IWU), Karlsruhe Institute of Technology (KIT), Germany.

MAARJA KRUUSMAA received the Ph.D. degree from the Chalmers University of Technology, in 2002. Since 2008, she has been a Professor with Tallinn University of Technology (TalTech) and a PI of the Centre for Biorobotics, a research group focusing on bio-inspired robotics, underwater robotics, and novel underwater sensing technologies. From 2017 to 2022, she was a Visiting Professor with the Centre for Excellence of Autonomous Marine Operations and Systems (AMOS), NTNU. Her research interests include novel locomotion mechanisms for underwater environments on flowable media and novel methods for underwater flow sensing.

ASKO RISTOLAINEN received the B.Sc. and M.Sc. degrees in mechatronics and the Ph.D. degree in information and communication technology from Tallinn University of Technology, Tallinn, Estonia, in 2008, 2010, and 2015, respectively. He is currently a Senior Researcher with the Centre for Biorobotics, School of Information Technologies, Tallinn University of Technology. His research interests include tactile and flow sensor design in robotics and remote environmental sensing.